Ribeiro *et al. EJNMMI Physics* (2026) 13:36
https://doi.org/10.1186/s40658-026-00850-y

EJNMMI Physics

ORIGINAL RESEARCH Open Access

Evaluation of the impact of low activity imaging in [^{11}C]-(+)-PHNO and [^{11}C]UCB-J PET-MR scans

Daniela Ribeiro[1*], William Hallett[2], Oliver Howes[3,4,5], Robert McCutcheon[3,4,5,6], Matthew M. Nour[3,6,7], David Nutt[5], David Erritzoe[5], Claudio Agnorelli[5] and Stephen Husbands[1]

*Correspondence:
Daniela Ribeiro
dfdfr20@bath.ac.uk; dfonseca92@gmail.com
[1]Department of Health, University of Bath, Bath, UK
[2]Perceptive, London, UK
[3]King's College London, London, UK
[4]Medical Research Council London, Institute of Medical Sciences, London, UK
[5]Imperial College London, London, UK
[6]Oxford University, Oxford, UK
[7]University College London, London, UK

Abstract

Introduction Positron Emission Tomography (PET) imaging is a close ally of Precision Medicine, and it has been proven to be indispensable in the field of Psychiatry. This imaging modality may also present an important role in understanding Neurodevelopmental disorders and their link to Psychiatric conditions, with new highly selective binders being used currently in research. PET imaging requires the administration of radiopharmaceuticals, where the radioisotope is in incorporated into a highly selective binder. Dosimetry and injected activity optimisation play a crucial role in the field of PET imaging as they allow to determine the radiation dose absorbed by target and non-target tissues, and determine the lowest amount required to deliver images with diagnostic quality and obtain reliable quantitative data, without overexposing patients. The aim of this research is to investigate the feasibility of reducing the injected activity of the [^{11}C]-(+)-PHNO and [^{11}C]UCB-J radiopharmaceuticals, for patients with neurodevelopmental disorders who undergo brain imaging in the PET-Magnetic Resonance (MR) scanner, without compromising quantitative accuracy of outcome measures.

Results No statistically significant differences were found when comparing the 1/2 to 1/6 datasets with the full injected activity [^{11}C]-(+)-PHNO dataset. Furthermore, the findings obtained from investigating the impact of low injected activity administrations of [^{11}C]UCB-J revealed that it is possible to reduce the administered activity by 1/2, when the clinical outcome measure under evaluation is the binding potential relative to non-displaceable volume (BP_{ND}). When the outcome measure under investigation is the standard uptake volume ratio (SUV_R), it is possible to decrease the injected activity to 1/3, for [^{11}C]UCB-J.

Conclusions The simulation and analysis methodologies deployed in this project are suitable for investigating scans with low injected activity for tracers with cortical and striatal uptake, when the outcome measure assessed is the BP_{ND} or the SUV_R. Whilst the data suggests that imaging with low injected activity is achievable, the efficacy of the investigation is highly dependent on the algorithm used to reconstruct the images, the outcome measure and the radiopharmaceutical used to acquire the PET-MR scans. For the [^{11}C]UCB-J radiopharmaceutical, it is possible to decrease the injectable activity to 1/3 of the original administration without compromising the SUV_R.

Keywords PET-CT, PET-MR, Injected activity reduction, Injected activity optimisation, Sustainability, Radiation protection

Background

Nuclear Medicine, and more specifically Positron Emission Tomography (PET), is an imaging modality which has been used in the field of Psychiatry with the aim of better understanding the aetiology of certain conditions and improving the quality of life of patients suffering from mental health illnesses [1].

In PET imaging, a highly selective binder designed to bind, with high affinity, to molecular targets is labelled with a radioisotope and administered to patients, with the aim to visualise and quantify target expression in vivo. The high sensitivity of these binders allows them to interact with biomolecules that are expressed or dysregulated in certain diseases or conditions and acquire imaging and quantitative PET data with high reliability. This data can, in turn, be used to stratify patients and select the most appropriate therapy, hence advancing precision medicine. The advance of Precision Medicine as an emerging approach which considers gene variability, environmental and lifestyles factors in the treatment and strategic prevention, has further established the role of PET imaging in the Psychiatric field [2, 3].

Whilst optimising the administered activity of radiopharmaceuticals is part of the "As Low As Reasonably Achievable" (ALARA) principals in diagnostic imaging, this is additionally important when conducting PET imaging in Psychiatry, as it is likely that younger individuals will be referred for imaging. Due to their developing tissues and greater cell division rate, young patients are more vulnerable to the effects of radiation, in comparison to adults. The risks arising from radiation exposure are cumulative and therefore may have an impact later in life [4].

Neurodevelopmental disorders (NDDs), in particular, are conditions arising from abnormal brain development and are often characterised by cognitive, communicative and/or behavioural impairments which may affect motor skills [5]. Symptoms related to NDDs have been described since the 18th century however, it wasn't until the mid-20th century that these disorders began to be classified as discrete entities [6]. Currently, the Diagnostic and Statistical Manual of Mental Disorders fifth edition (DSM-5) recognises conditions within the autism spectrum disorder (ASD), attention deficit hyperactivity disorder (ADHD) and intellectual disability (ID) as NDDs [7].

Evidence however suggests that childhood neurodevelopmental disorders appear to share specific genetic alleles not only with each other but also with psychiatric disorders, with emerging data proposing that there may be pathogenic mechanisms which overlap between ID, ASD and ADHD and bipolar disorder (BPD) and schizophrenia [6]. Moreover, people suffering from NDDs present higher rates of psychiatric morbidity [7].

Imaging patients at earlier timepoints may allow a better understanding of the aetiology of NDDs, and longitudinal imaging may offer insights into the pathogenic mechanisms overlapping between NDDs and psychiatric conditions. Optimisation of injected activities should, therefore, be considered and addressed in psychiatric populations due to the young age of the participants and the potential longitudinal examinations they may require follow-up on the disease process and therapeutic efficacy [8].

The aim of this study was to investigate the feasibility of reducing the injected activity of radiopharmaceuticals in patients with neurodevelopmental disorders who undergo brain imaging in the PET-MR scanner, without compromising quantitative accuracy of outcome measures. To address this, PET-MR datasets with the full injected activity were compared to simulated datasets with low injected activity, and the accuracy of two clinical outcomes measures were assessed through statistical tests.

Methods

A retrospective analysis was performed on data acquired from two academic research studies. Study 1, required the administration of (4aR,10bR)-4-propyl-3,4,4a,5,6,10b-hexahydro-2 H-naphtho[1,2-b] [1, 4] oxazin-9-ol ([^{11}C]-(+)-PHNO) which is a radiopharmaceutical that binds to D2 and D3 receptors in the brain [9]. [^{11}C]-(+)-PHNO can be used as a surrogate for measuring extracellular dopamine changes, with its normal biodistribution in the brain including the substantia nigra, hypothalamus, ventral striatum, globus pallidus and thalamus [10, 11]. Study 2, required the administration of (4R)-1-{[3-(^{11}C)Methylpyridin-4-yl]methyl}-4-(3,4,5-trifluorophenyl)pyrrolidin-2-one ([^{11}C]UCB-J) which is a radiopharmaceutical that binds to the synaptic vesicle glycoprotein 2 A in the brain [12]. [^{11}C]UCB-J can be used as a marker for synaptic loss, with its normal biodistribution in the brain including the thalamus, ventral striatum, caudate, insula, parietal lobe and frontal cortex [13]. In both studies, counts were acquired dynamically over 90 min, and binned into 31 frames (duration: 8 × 15s, 3 × 60s, 5 × 120s, 15 × 300). This process allows for the evolution of the tracer to be preserved, ensuring the shorter initial frames capture the early phase of the radiopharmaceutical and the longer later frames capture the slower biological phase of the tracer distribution, even during the low activity simulations.

Neither of these radiopharmaceuticals is currently being used in clinical practice. This is mainly due to the short half-life of carbon-11, which does not allow them to be transported as they decay too rapidly.

Both studies adhered to the principles outlined in the National Health Service (NHS) Research Governance Framework for Health and Social Care (2nd edition), the Declaration of Helsinki and Good Clinical Practice (GCP). The data used in this project was acquired after the participants' consent was obtained for the original study. Use of this data was covered in the original consent form, which stated that the data acquired could be used in future related research and written permission was obtained from both Chief Investigators.

[^{11}C]-(+)-PHNO PET-MR datasets

Datasets from 10 adult healthy participants who had received [^{11}C]-(+)-PHNO were retrieved for re-reconstruction and analysis. The average age of the participants was 22.4 years with the female to male ratio being 6:4. The mean administered activity was 134.2 ± 20.3 MBq (mean ± SD, $n = 10$).

The ZTE sequence was acquired and used for attenuation correction of the PET images. The T1-weighted images were acquired as Bravo sequences, to assist with image analysis.

[^{11}C]UCB-J PET-MR datasets

Datasets from 5 healthy adult participants who had received [^{11}C]UCB-J were retrieved for re-reconstruction and analysis. The average age of the participants was 38.6 years, with only males participating in the study. The mean administered activity was 228.6 ± 58.3 MBq (mean ± SD, $n = 5$).

The ZTE sequence was acquired and used for attenuation correction of the PET images. The T1-weighted images were acquired as fast spoiled gradient-echo (FSPGR) sequences, to assist with image analysis.

Low data simulations and reconstructions

As the original data was acquired in a list-mode format, low-activity datasets were generated by introducing delays at the start of each frame and re-reconstructing the data contained within the last section of each frame. This approach ensured that the data binned at the start of the frame was consistently rejected and the data binned at the end of the frames was consistently included.

Seven low activity simulations were simulated: 1/2, representing 50%; 1/3, representing 33%; 1/4, representing 25%; 1/5, representing 20%; 1/6, representing 16.66%; 1/10, representing 10%; and 1/15 representing 6.67% of the original administered activity. The simulated data was binned according to the framework indicated in Table 1:

Simulating dose reduction by introducing delays reflects realistic clinical conditions in which a reduced administered activity results in a lower number of detected coincidences. This strategy allows for the statistical and temporal characteristics of the scanner to be maintained. Moreover, this method allows use of the standard clinical reconstruction workflow without the need for dedicated list-mode manipulation tools, thereby guaranteeing that the methodology deployed can be reproduced in different scanners.

All PET data was reconstructed with a display field of view (DFOV) of 30 cm and a matrix of 192 × 192. An OSEM algorithm with time-of-flight information (TOF) denominated VPFXS was used with 6 iterations, 16 subsets, a 5 mm filter in the xy-axis and no filter in the z-axis.

Image analysis

For the [^{11}C]-(+)-PHNO datasets, the impact of the low activity simulations was investigated on the binding potential relative to non-displaceable volume (BP_{ND}) outcome measure for the striatum, caudate, putamen, globus pallidus, thalamus, substantia nigra, accumbens and cerebellum. A single reference tissue model (SRTM) with the cerebellum as a reference region was used. This was due to the cerebellum representing a region of the brain devoid of receptors that would bind to [^{11}C]-(+)-PHNO [14].

Table 1 Frame and duration scheme to simulate low activity datasets

	Start of the acquisition	→		End of the acquisition
Full activity	8 frames x 15 s	3 frames x 60 s	5 frames x 120 s	15 frames x 300 s
1_2_LowActivity	8 × 7s (8s delay)	3 × 30s (30s delay)	5 × 60s (60s delay)	15 × 150s (150s delay)
1_3_LowActivity	8 × 5s (10s delay)	3 × 20s (40s delay)	5 × 40s (80s delay)	15 × 100s (200s delay)
1_4_LowActivity	8 × 4s (11s delay)	3 × 15s (45s delay)	5 × 30s (90s delay)	15 × 75s (225s delay)
1_5_LowActivity	8 × 3s (12s delay)	3 × 12s (48s delay)	5 × 24s (96s delay)	15 × 60s (240s delay)
1_6_LowActivity	8 × 2s (13s delay)	3 × 10s (50s delay)	5 × 20s (100s delay)	15 × 50s (250s delay)
1_10_LowActivity	8 × 1s (14s delay)	3 × 6s (54s delay)	5 × 12s (108s delay)	15 × 30s (270s delay)
1_15_LowActivity	8 × 1s (14s delay)	3 × 4s (56s delay)	5 × 8s (112s delay)	15 × 20s (280s delay)

For the [^{11}C]UCB-J datasets, the impact of the low activity simulations was investigated on the BP_{ND} and Standard Uptake Volume ratio (SUV_R) outcome measures for the brainstem, substantia nigra, thalamus, striatum, caudate, putamen, hippocampus, insular cortex, temporal lobe, parietal lobe, frontal cortex, cerebellum and accumbens. A SRTM model with the centrum semiovale as reference region was used. This was due to the low binding of [^{11}C]UCB-J to white matter and previous research having determined that the centrum semiovale is a suitable pseudo reference region [13].

All images were analysed using a PET quantification software denominated MIAKAT. The pipeline follows a sequence of steps namely brain extraction (using MATLAB and FSL functions), brain segmentation (using SPM12 function), motion correction, region of interest (ROI) definition, ROI tracer kinetic modelling and parametric imaging. The outputs of each step were reviewed and manually accepted by the investigator.

Data analysis

Descriptive statistics were calculated for each structure, per simulation. Similarly, the coefficient of variation (CV) (which indicates the dispersion of the data acquired for all participants in relation to the mean, per dataset, per brain structure), Bland-Altman plots (which demonstrate the relationship between the full activity-simulation paired variables, per brain structure) and bias (which indicates the difference between the outcome measure obtained from the simulation and the outcome measure from the full activity dataset, per brain structure) were also calculated [15, 16]. These statistics were calculated using the GraphPad Prism version 9 software. Normality and Homogeneity of variance were investigated with the Shapiro Wilko and Levene's test, respectively. The ANOVA with Bonferroni multicomparisons and the Kruskal-Wallis tests were used to investigate statistically significant differences. These were performed using IBM SPSS Statistics software, version 29.0.1.1.

Results

Findings of low activity [^{11}C]-(+)-PHNO on BP_{ND}

The analysis of the coefficient of variation (CV) revealed that the substantia nigra and the thalamus presented the highest values for the Full activity datasets (20.55% and 39.90%, respectively). The CVs, for the Full activity datasets of all other structures were below 20%, as presented in Supplementary Table 1. A summary display of the CVs is present in Fig. 1.

When investigating the bias (as an absolute measure) present in the low activity simulations, it was noted that the 1/10 and the 1/15 low activity simulations consistently produced the highest bias for all structures. The 1/2 and 1/3 low activity simulations produced the lowest bias for the caudate, globus pallidus and thalamus. For the accumbens, putamen, striatum and substantia nigra, the 1/5 simulation produced the lowest bias, as indicated in Table 2.

Out of all the structures investigated, the substantia nigra and the thalamus were the only ones that did not follow a normal distribution. Moreover, with the exception of the putamen and the striatum, no statistically significant differences were observed when comparing the 1/2, 1/3, 1/4, 1/5, 1/6 low activity simulations with the Full activity dataset.

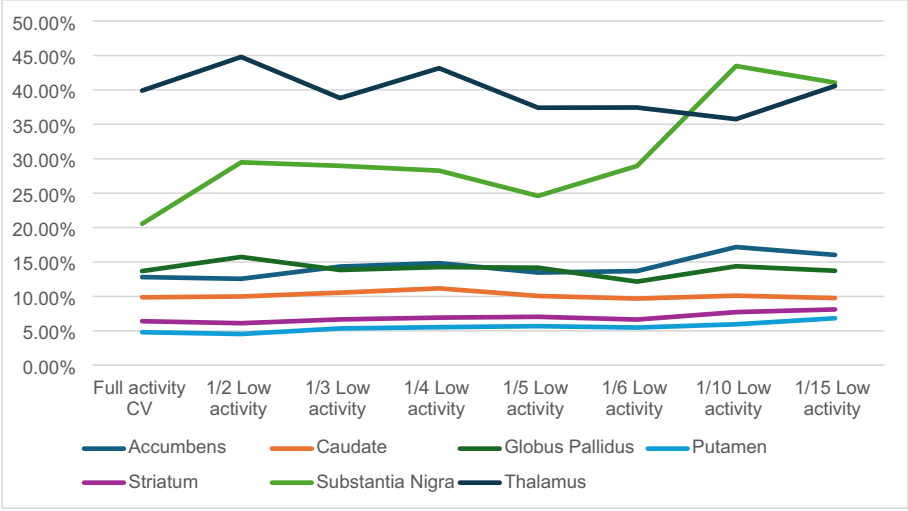

Fig. 1 Summary display of the coefficients of variation (CVs) obtained for the low activity [11 C]-(+)-PHNO on BPND

Table 2 Bias calculated between the low activity simulated datasets and the full activity datasets, when investigating the impact of low activity [^{11}C]-(+)PHNO on BP_{ND}

	1/2 Low activity	1/3 Low activity	1/4 Low activity	1/5 Low activity	1/6 Low activity	1/10 Low activity	1/15 Low activity
Accumbens	-0.049	0.059	0.054	0.036	0.106	0.238	0.328
Caudate	-0.050	-0.005	0.012	0.046	0.051	0.132	0.170
Globus Pallidus	0.009	0.069	0.017	0.154	0.143	0.251	0.387
Putamen	-0.050	-0.020	-0.023	-0.006	0.018	0.058	0.119
Striatum	-0.053	-0.013	-0.011	0.012	0.035	0.103	0.155
Substantia Nigra	0.028	0.030	0.031	0.022	0.077	0.082	-0.057
Thalamus	-0.029	-0.016	-0.043	-0.019	-0.030	-0.030	-0.032

Figure 2 plots the outcome measure for the [^{11}C]-(+)-PHNO on the y axis (the BP_{ND} parameter) against the activity simulations on the x axis (1 is the equivalent to the Full activity dataset and 0.2 is the equivalent to the 1/5 low activity simulation), for the Caudate.

The data indicates that above 50% of the injected activity, there is no correlation between the outcome measure (BP_{ND}) and the simulation performed, for the [^{11}C]-(+)-PHNO. However, below this threshold, the outcome measure appears to decrease with the injected activity. Moreover, the graph also shows a significant decrease in the value of the outcome measure for simulations mimicking significant low activity scenarios, such as the 1/10 and the 1/15 simulations.

Findings of low activity [^{11}C]UCB-J on BP_{ND}

During the analysis of the coefficient of variation (CV) it was noted that the cerebellum and the substantia nigra presented the highest values for the Full activity datasets (25.47% and 134.80%, respectively). The CVs, for the Full activity datasets of all other structures were below 20%, as presented in Supplementary Table 2. A summary display of the CVs is present in Fig. 3.

When investigating the bias present in the low activity simulations, it was noted that the 1/15 low activity simulations produced the highest bias for all structures, with the

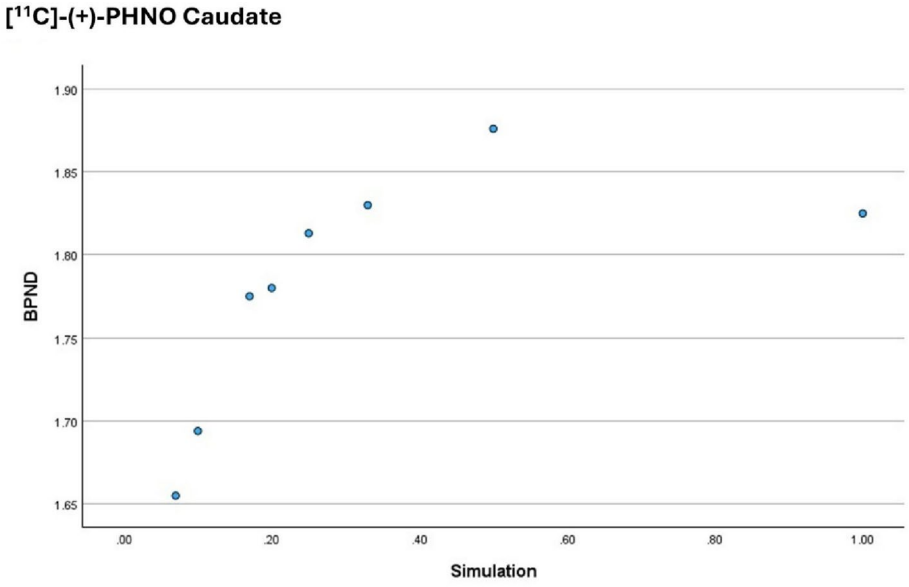

Fig. 2 BP_{ND} obtained from the [^{11}C]-(+)-PHNO in the Caudate, per activity simulation. The graph demonstrates that there is no correlation between the dependent variable and the independent variable

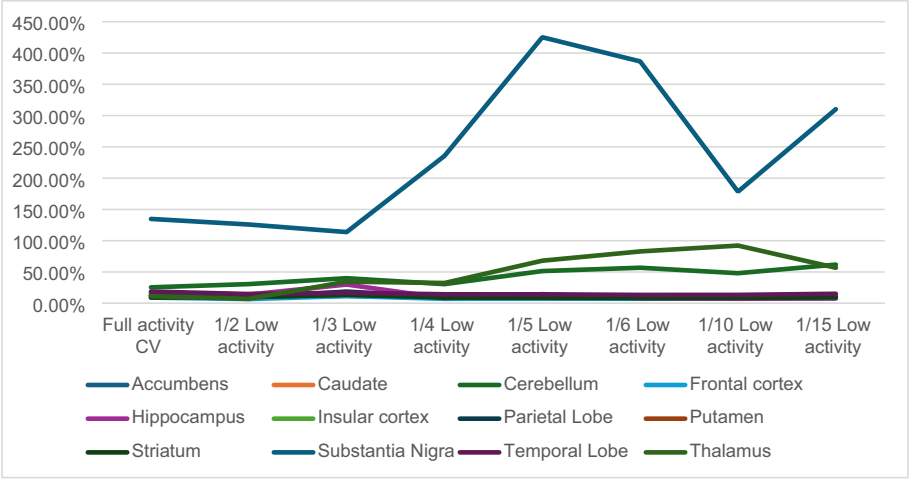

Fig. 3 Summary display of the coefficients of variation (CVs) obtained for the low activity [11 C]UCB-J on BPND

exception of the thalamus. For the thalamus, the 1/6 low activity simulations produced the highest bias of 0.939, closely followed by the 1/10 and 1/15 low activity simulations with biases of 0.937 and 0.541, respectively. The 1/2 and 1/3 low activity simulations produced the lowest bias for all structures (Table 3).

Out of all the structures investigated, the hippocampus, putamen, substantia nigra and thalamus were the ones that did not follow a normal distribution. No statistically significant differences were found when comparing the 1/2 low activity with the full activity datasets, for all the structures, as indicated in Fig. 4.

Moreover, with the exception of the accumbens, the remaining brain structures also did not reveal any statistically significant differences when the 1/3 low activity and the full activity datasets were compared.

Table 3 Bias calculated between the low activity simulated datasets and the Full activity datasets, when investigating the impact of low activity [^{11}C]UCB-J on BP_{ND}

	1/2 Low activity	1/3 Low activity	1/4 Low activity	1/5 Low activity	1/6 Low activity	1/10 Low activity	1/15 Low activity
Accumbens	0.453	0.670	0.867	1.045	1.152	1.358	1.536
Caudate	0.154	-0.065	0.320	0.394	0.523	0.653	0.826
Cerebellum	0.166	0.468	0.536	0.735	0.815	0.851	1.037
Frontal cortex	0.232	0.290	0.450	0.547	0.604	0.720	0.878
Hippocampus	-0.046	0.162	0.532	0.686	0.822	0.888	1.008
Insular cortex	0.100	0.601	0.726	0.884	0.952	1.113	1.248
Parietal Lobe	0.287	0.271	0.568	0.677	0.758	0.869	1.006
Putamen	0.207	0.284	0.478	0.634	0.731	0.871	1.035
Striatum	0.208	0.234	0.453	0.588	0.690	0.834	1.002
Substantia Nigra	0.133	0.182	0.345	0.334	0.641	0.649	0.809
Temporal Lobe	0.130	0.540	0.664	0.804	0.867	1.052	1.193
Thalamus	0.126	0.351	0.419	0.817	0.939	0.937	0.541

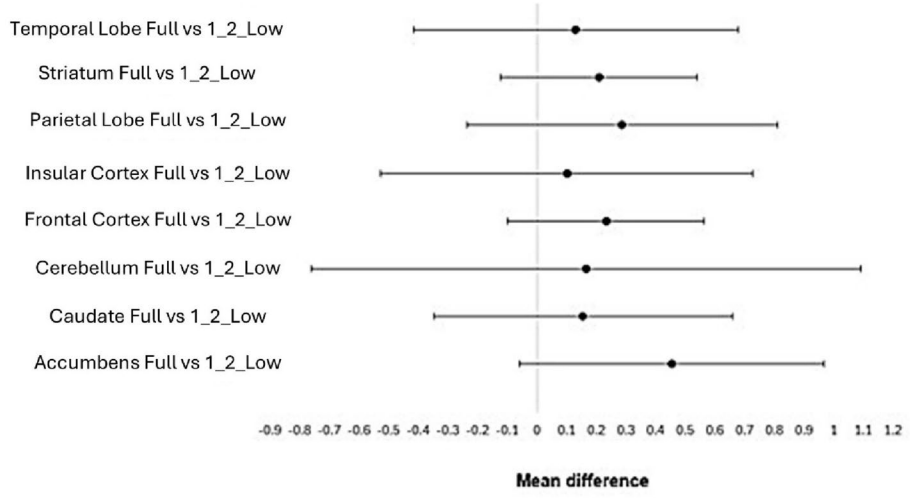

Fig. 4 Visual representation of no statistically significant differences present when comparing the Full activity dataset with the 1/2 low activity dataset, for the parametric data

Figure 5 plots the outcome measure for the [^{11}C]UCB-J on the y axis (the BP_{ND} parameter) against the activity simulations on the x axis (1 is the equivalent to the Full activity dataset and 0.2 is the equivalent to the 1/5 low activity simulation), for the Parietal lobe.

The plot indicates that above 33% of the injected activity, there is no correlation between the outcome measure (BP_{ND}) and the simulation performed, for the [^{11}C]UCB-J. Below this threshold, the outcome measure appears to decrease with the injected activity, for this radiopharmaceutical.

Findings of low activity [^{11}C]UCB-J on SUV_R

During the analysis of the coefficient of variation (CV) it was found that none of the structures presented variations above 15% (as indicated in Supplementary Table 3). A summary display of the CVs is present in Fig. 6. The structures with the highest CVs for the full activity datasets were the caudate (10.21%), cerebellum (11.21%), substantia nigra (10.68%) and temporal lobe (10.25%).

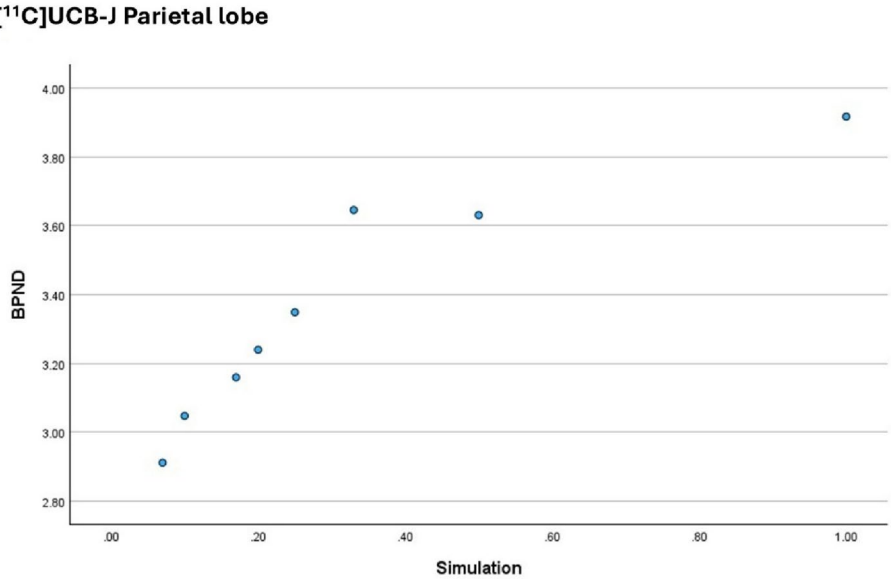

Fig. 5 BP_{ND} obtained from the [^{11}C]UCB-J in the Parietal lobe, per activity simulation. The graph demonstrates that there is no correlation between the dependent variable and the independent variable

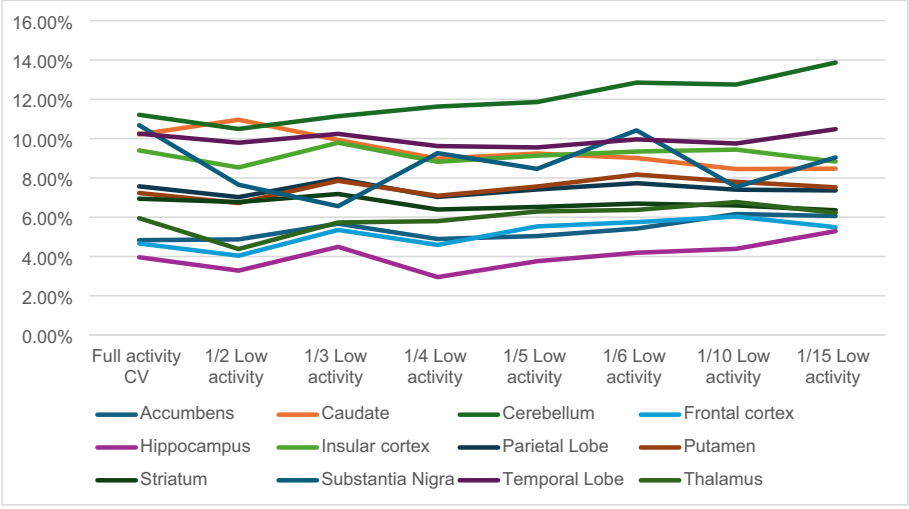

Fig. 6 Summary display of the coefficients of variation (CVs) obtained for the low activity [11 C]UCB-J on SUVR

An analysis of the bias revealed that the 1/2 low activity simulation consistently produced the lowest bias for all structures (Table 4). With the exception of the substantia nigra, the highest bias for the remaining structures was found with the 1/15 low activity simulation. For the substantia nigra, the highest bias was found in the 1/10 low activity dataset (0.076), with the second highest bias being the one obtained in the 1/15 low activity dataset (0.074). Similarly to what was found when examining the bias obtained for the [^{11}C]UCB-J BP_{ND}, the less counts will be available in the brain structures, and the higher the bias will be.

Out of all the structures investigated, the striatum and the temporal lobe were the only ones that did not follow a normal distribution. No statistically significant differences were found when comparing the 1/2 and 1/3 low activity datasets with the full activity datasets, for all the structures, as indicated in Figs. 7 and 8 respectively.

Table 4 Bias calculated between the low activity simulated datasets and the full activity datasets, when investigating the impact of low activity [^{11}C]UCB-J on SUV_R

	1/2 Low activity	1/3 Low activity	1/4 Low activity	1/5 Low activity	1/6 Low activity	1/10 Low activity	1/15 Low activity
Accumbens	0.017	0.086	0.159	0.263	0.318	0.433	0.555
Caudate	0.031	0.106	0.157	0.262	0.324	0.437	0.598
Cerebellum	0.031	0.090	0.158	0.203	0.233	0.310	0.409
Frontal cortex	0.017	0.089	0.137	0.228	0.273	0.360	0.484
Hippocampus	0.006	0.079	0.106	0.209	0.260	0.296	0.387
Insular cortex	0.014	0.084	0.137	0.229	0.271	0.368	0.481
Parietal Lobe	0.018	0.082	0.133	0.227	0.279	0.352	0.472
Putamen	0.024	0.113	0.173	0.296	0.362	0.465	0.599
Striatum	0.025	0.106	0.165	0.279	0.341	0.450	0.591
Substantia Nigra	0.027	0.031	0.066	0.047	0.076	0.076	0.074
Temporal Lobe	0.011	0.075	0.133	0.211	0.249	0.346	0.463
Thalamus	0.026	0.081	0.105	0.167	0.203	0.225	0.269

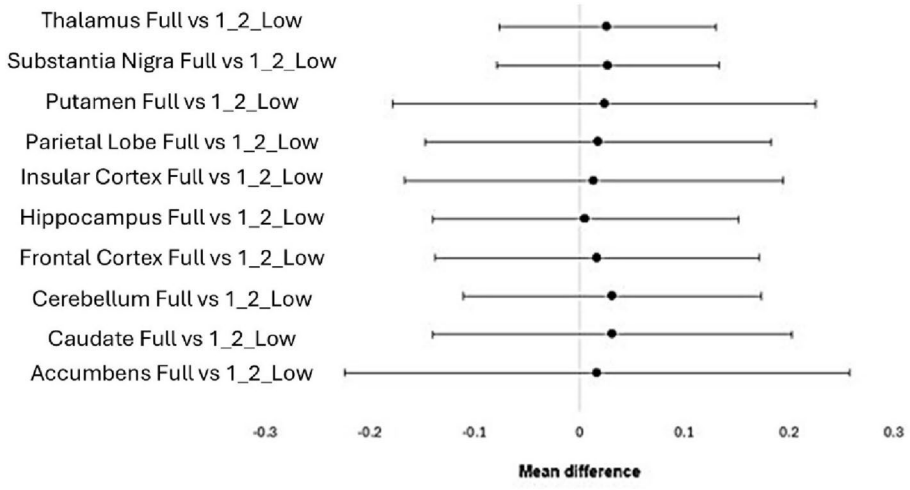

Fig. 7 Visual representation of no statistically significant differences present when comparing the Full activity dataset with the 1/2 low activity dataset, for the parametric data

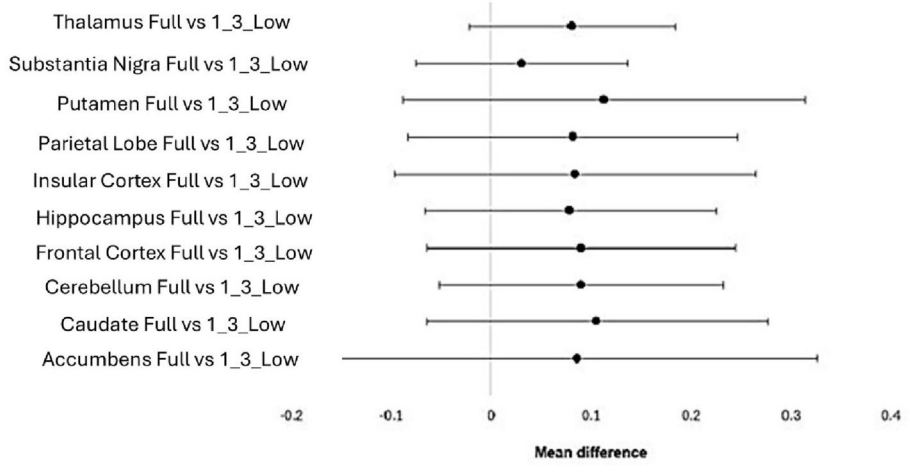

Fig. 8 Visual representation of no statistically significant differences present when comparing the full activity dataset with the 1/3 low activity dataset, for the parametric data

Moreover, with the exception of the cerebellum and the thalamus, the remaining brain structures also did not reveal any statistically significant differences when the 1/4 low activity and the full activity datasets were compared.

Figure 9 plots the outcome measure for the [^{11}C]UCB-J on the y axis (the SUV_R parameter) against the activity simulations on the x axis (1 is the equivalent to the Full activity dataset and 0.2 is the equivalent to the 1/5 low activity simulation), for the Parietal lobe.

The plot indicates that above 33% of the injected activity, there is no correlation between the outcome measure (SUV_R) and the simulation performed, for the [^{11}C]UCB-J. Below this threshold, the outcome measure appears to decrease with the injected activity, for this radiopharmaceutical.

Discussion

Impact of low activity [^{11}C]-(+)-PHNO on BP_{ND}

Small structures, such as the substantia nigra, are more susceptible to low activity simulations, particularly those in which the number of counts is significantly reduced. Whilst the transaxial spatial resolution of the GE SIGNA PET-MR scanner is of the order of 4 mm near the centre of the field of view, the substantia nigra is a small structure with a thickness of 5.1 ± 0.89 mm noted in health volunteers [17, 18]. Therefore, the visibility of such a small structure will be substantially impacted by the amount of radiopharmaceutical administered and the movement during scan acquisition.

In the case of the thalamus, when simulating low activity scenarios of 1/2, 1/3, 1/4, 1/5, 1/6, 1/10 and 1/15, the CV ranged between a minimum of 35.75% and a maximum of 44.79%. In comparison to the CV obtained for the Full activity dataset, this variation only equated to a difference of a maximum of approximately 5%, which can be accepted when conducting these simulations. This, however, demonstrates that the high CV is not related to the simulation method itself but rather with the brain structure under investigation and the radiopharmaceutical uptake. Figure 10 demonstrates the uptake of [^{11}C]-(+)-PHNO in the brain, across the low activity datasets.

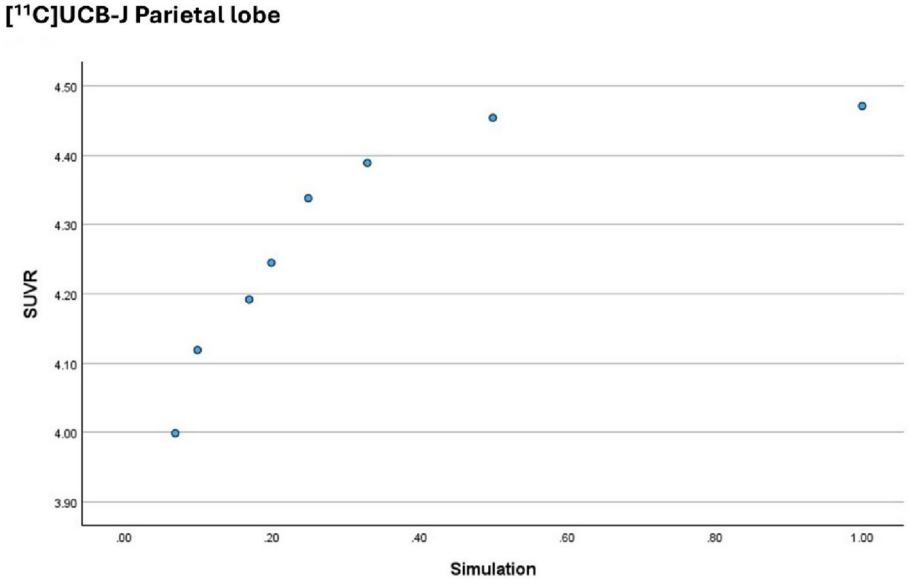

Fig. 9 SUV_R obtained from the [^{11}C]UCB-J in the Parietal lobe, per activity simulation. The graph demonstrates that there is no correlation between the dependent variable and the independent variable

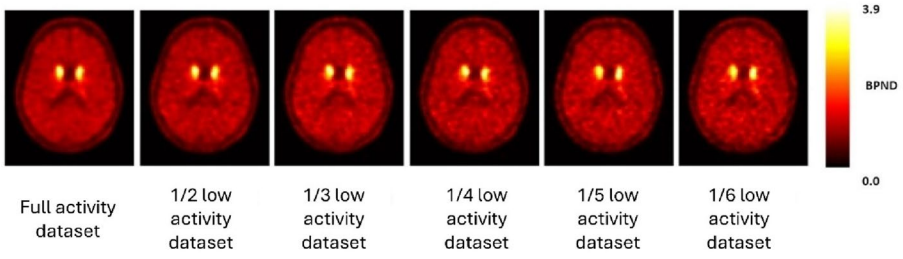

Fig. 10 BP_{ND} axial images representative of the full dataset and low dose datasets, 1/2 to 1/6

In the case of the putamen, the 1/5 simulation produced the smallest bias, followed by the 1/6, 1/3, 1/4 and 1/2 simulations. A similar pattern was noted in the striatum, with the 1/4 simulation producing the smallest bias, followed by the 1/5, 1/3, 1/6 and 1/2 simulations. Although the putamen and the striatum presented statistically significant differences when comparing the 1/2, 1/10 and 1/15 with the Full activity datasets, a visual inspection of the graphics in Fig. 8 reveals that there is minimal to no change in the shape of the time activity curves for the 1/2 low activity and the Full activity datasets (Fig. 11).

Impact of low activity [^{11}C]UCB-J on BP_{ND}

In the case of the cerebellum, when simulating low activity scenarios of 1/2, 1/3 and 1/4, the CV ranged between a minimum of 30.60% up to a maximum of 40.07%. In comparison to the CV obtained for the Full activity dataset, this variation equated to a difference of a maximum of 14.6%. When simulating low activity scenarios of 1/5, 1/6, 1/10 and 1/15, the CV ranged between a minimum of 48.06% and a maximum of 61.82%, in comparison with the full activity dataset. This variation equated to a difference of a maximum of 36.35%. This demonstrates that the wider variability is related to the brain structure itself and the uptake of the radiopharmaceutical in the region, and that this effect is exacerbated under very low activity simulations.

In the case of the substantia nigra, the CV results obtained appear to be skewed, affecting not only the low activity simulation datasets but also in the full activity dataset. The minimum BP_{ND} values obtained for all the datasets (low activity and full activity) are negative. This is further substantiated by the fact that the CV obtained for the full activity dataset was of the order of 134.8%, and the CVs obtained for the 1/2 to 1/15 simulations range between a minimum of 113.8% to maximum of 425.2%.

These findings prompted a more in-depth review of the BP_{ND} data obtained for each participant, at each low activity simulation. Whilst a negative outcome measure can potentially be present for low activity datasets due to the lack of sufficient counts in the brain regions, the BP_{ND} should never be negative for the full activity datasets. The data review revealed that, for two out of the five participants, the BP_{ND} obtained for the full activity dataset was negative. If the data from these participants had been removed, then the overall CV of the Full activity dataset would drop to 17.11% and the CV for the 1/2 activity simulation would drop to 49.74%. Additionally, for the Full activity and the 1/2 activity datasets, the minimum BP_{ND} value would also remain positive. The CV for the 1/3 to 1/15 low activity simulations would, however, remain high.

Figure 12 presents the time activity curves, for all the low activity simulations and the full activity dataset, for the cerebellum, substantia nigra, hippocampus and thalamus.

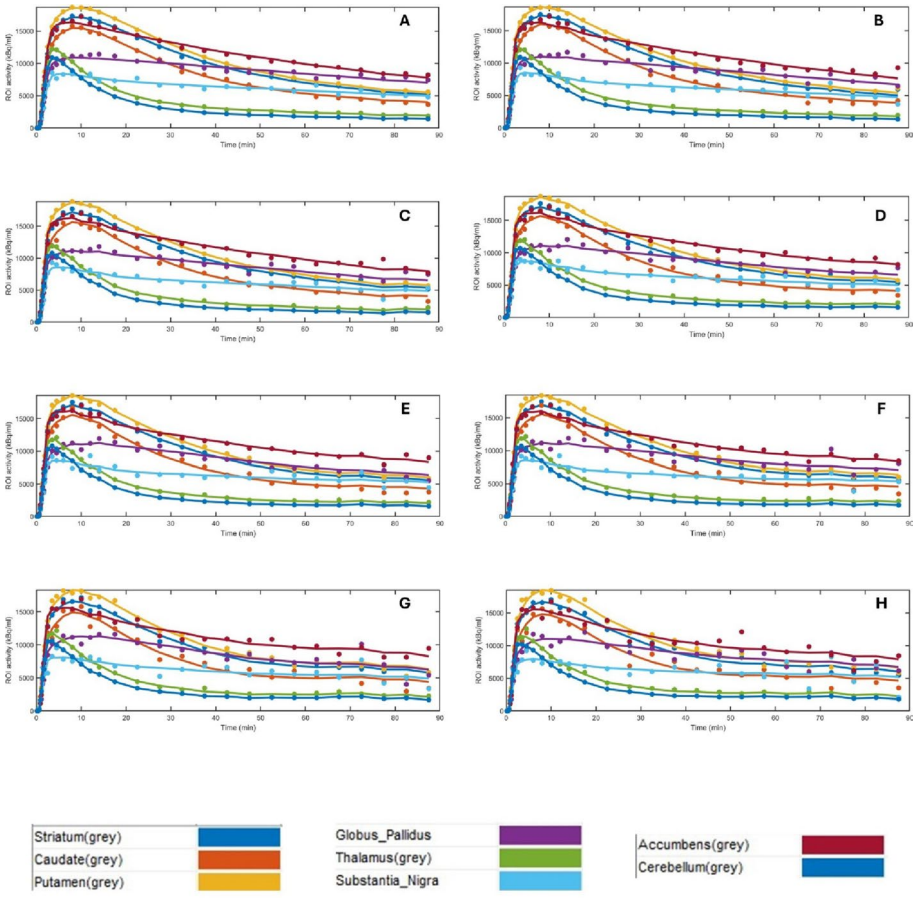

Fig. 11 Time activity curves (TACs) obtained for the striatum, caudate, putamen, globus pallidus, thalamus, substantia nigra and accumbens, for one participant dataset. **A**- TACs from those datasets representative of Full activity. **B**- TACs those datasets representative of 1/2 of the administered activity. **C**- TACs those datasets representative of 1/3 of the administered activity; **D**- TACs those datasets representative of 1/4 of the administered activity; **E**- TACs those datasets representative of 1/5 of the administered activity; **F**- TACs those datasets representative of 1/6 of the administered activity; **G**- TACs those datasets representative of 1/10 of the administered activity; **H**- TACs those datasets representative of 1/15 of the administered activity

In the case of the hippocampus, the CV obtained for the 1/2 low activity dataset is very similar to that of the full activity dataset (13.92% and 17.18%, respectively). However, for the 1/6, 1/10 and 1/15 low activity datasets, there is a substantial decrease of the CV (8.07%, 7.22% and 8.08%, respectively). This drop in CV may be due to difficulty in identifying counts in the hippocampus, when the activity is significantly reduced. The thalamus, however, displays the opposite case to that observed for the hippocampus. Whilst the 1/2 low activity and Full activity datasets present very similar CVs (7.08% and 11.42%, respectively), there is a substantial increase in CVs when the 1/3, 1/4, 1/5, 1/6, 1/10 and 1/15 simulations are performed (34.52%, 32.41%, 68.06%, 82.85%, 92.21% and 56.80%, respectively).

Impact of low activity [^{11}C]UCB-J on SUV_R

The highest CVs detected were in line with those observed for the [^{11}C]UCB-J BP_{ND} results, as both the cerebellum and substantia nigra had been noted as having the highest CVs, for the full activity datasets. This further sustains the premise that the wider variability is partially related to the brain structures themselves and the radiopharmaceutical

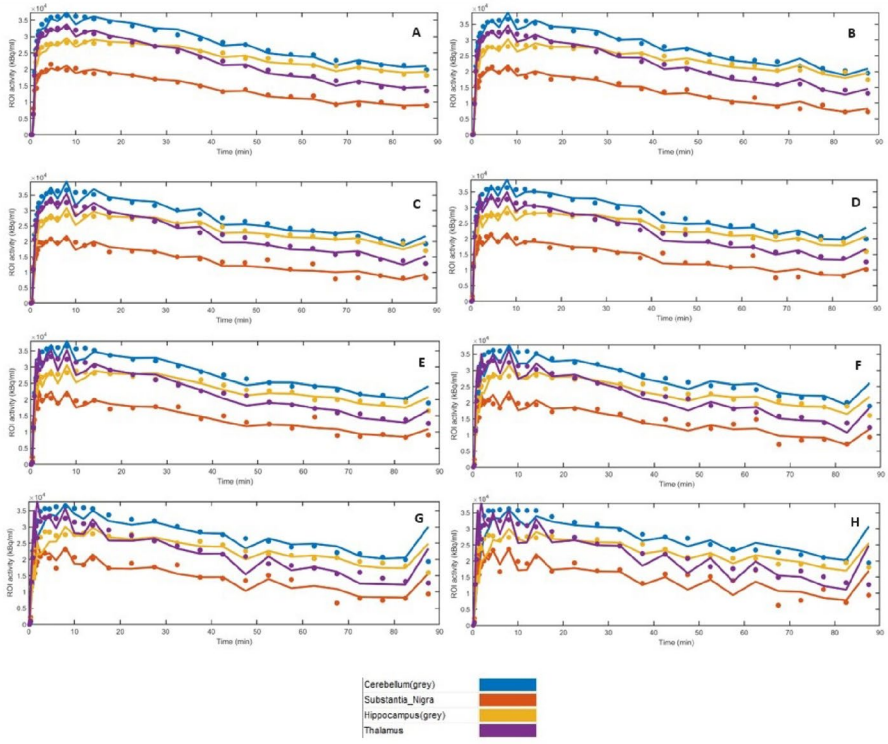

Fig. 12 Time activity curves (TACs) obtained for the cerebellum, substantia nigra, hippocampus and thalamus, for one participant. **A**- TACs from those datasets representative of Full activity. **B**- TACs those datasets representative of 1/2 of the administered activity. **C**- TACs those datasets representative of 1/3 of the administered activity; **D**- TACs those datasets representative of 1/4 of the administered activity; **E**- TACs those datasets representative of 1/5 of the administered activity; **F**- TACs those datasets representative of 1/6. **G**- TACs those datasets representative of 1/10; **H**- TACs those datasets representative of 1/15 dataset

uptake in that region. The low CVs obtained for the full activity datasets demonstrate that there is less variability around the mean of the SUV_R, suggesting the stability and reliability of this outcome measure.

Figure 13 presents the SUV_R parametric images for the full activity, 1/2 and 1/15 low activity datasets

Moreover, when analysing the range of the CVs obtained for all the low activity simulations, none of the structures presented variations above 4%. The structures with the highest variation of CVs for the low activity simulations were the substantia nigra (3.86%), cerebellum (3.38%), caudate (2.51%) and thalamus (2.39%). This finding is also in line with that observed for the [^{11}C]UCB-J BP_{ND} results, as the cerebellum and substantia nigra had been noted as having the highest variation of CVs, for the low activity datasets. Overall, the low CVs obtained when the various regimens of the low activity datasets are compared, further sustains the premise that the SUV_R is a robust outcome measure when investigating low activity scenarios.

Overall discussion

When comparing the low activity simulations and BP_{ND} analysis conducted for the [^{11}C]-(+)-PHNO datasets with that which was conducted for the [^{11}C]UCB-J, it can be understood that the methodology worked best in the latter dataset. In the [^{11}C]UCB-J BP_{ND} analysis there was a consistent tendency for the 1/2 and/or 1/3 low activity simulations to produce the lowest bias. With the [^{11}C]-(+)-PHNO BP_{ND} analysis however, this

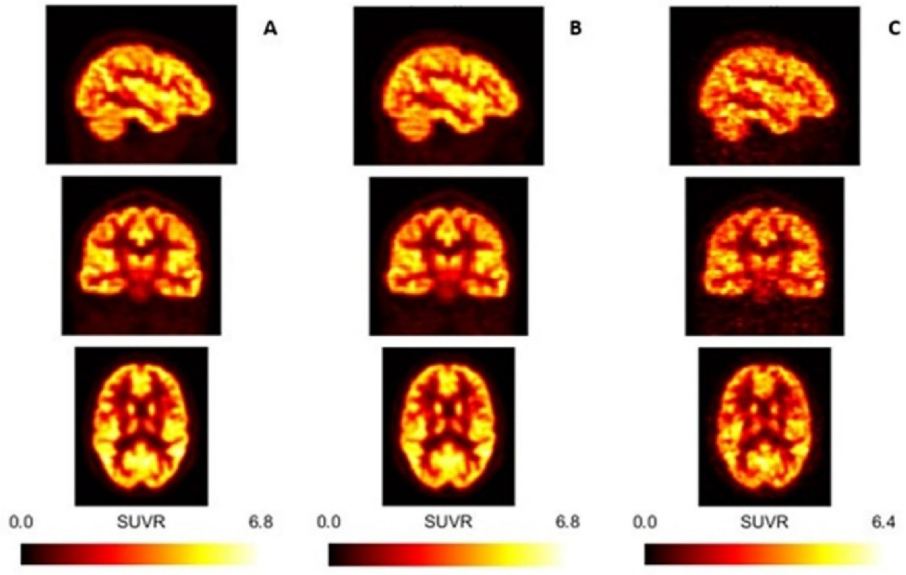

Fig. 13 SUV_R images obtained from three different datasets from the same participant (the top images are sagittal views; the middle images; are coronal views and the lower images are axial views). Dataset A is representative of the Full activity dataset; dataset B is representative of the 1/2 low activity dataset; dataset C is representative of the 1/15 low activity dataset.

pattern was not predominant. Whilst some structures did show the above pattern, the putamen and striatum were clear outliers. Similarly, whilst the [^{11}C]UCB-J BP_{ND} analysis did not reveal any statistically significant differences when the 1/2 low activity simulation was compared to the full activity dataset, there were structures within the [^{11}C]-(+)-PHNO BP_{ND} analysis that revealed statistically significant differences for the same comparison.

Additionally, when comparing the low activity simulations and outcome measures for the [^{11}C]UCB-J BP_{ND} and [^{11}C]UCB-J SUV_R analysis, it can be perceived that the methodology worked best in the later. Whilst in the BP_{ND} analysis there was a tendency for the 1/2 and/or 1/3 low activity simulations to produce the lowest bias, in the SUV_R the 1/2 low activity simulation consistently produced the lowest bias for all structures. Similarly, whilst the BP_{ND} analysis did not reveal any statistically significant differences when the 1/2 low activity simulation was compared to the Full activity dataset, the SUV_R analysis did not reveal any statistically significant differences when the Full activity dataset was compared to the 1/2 and 1/3 low activity simulations. It is therefore hypothesised that the simulation and analysis methodologies used in this study are best suited when investigating SUV_R, rather than BP_{ND}.

Conclusion

Whilst the data suggests that the efficacy of the investigation is highly dependent on the algorithm used to reconstruct the images, the outcome measure and the radiopharmaceutical, it can be assumed that the methodology used is well suited for investigating low activity scans for tracers with cortical and striatal uptake, when the outcome measure assessed is the BP_{ND} or the SUV_R.

Importantly, for the [^{11}C]UCB-J radiopharmaceutical, the data shows data the injectable activity can be decreased to 1/3 of the original administered activity, without a compromise to the clinical outcome measure SUV_R.

Activity optimisation and low activity imaging are aligned with the principles of justification and optimisation from the ALARA and "As Low as Reasonably Practicable" (ALARP) guidance, as well as the recommendations of the International Commission on Radiological Protection (ICRP) [19, 20]. Moreover, activity optimisation and low activity imaging are intrinsically related with sustainability and, as Currie et al. (2024) indicated, the optimisation of acquisition protocols is a potential approach for fostering environmental sustainability [21]. In the case of radiopharmaceuticals specifically produced for research purposes, ensuring their sustainable production and consumption, in central and local radiopharmacies, is directly related with the United Nations' Sustainable Development Goal (SDG) 12 – Responsible consumption and production. Taking action to combat climate change and its impacts, through optimising and justifying Nuclear Medicine procedures is in line with SDG 13 – Climate change [22].

Additionally, low activity imaging is also related to social sustainability. Ensuring the healthy lives and promoting well-being of patients (particularly those living with Neurodevelopmental disorders), carers and family members who attend nuclear medicine examinations, through a reduction in radiopharmaceutical administration and radiation exposure is directly correlated with the SDG 3 – Good health and well-being. Similarly, promoting the well-being of professionals who work within the field of Nuclear Medicine, through a decrease of occupational exposure levels is directly correlated with this SDG.

The authors acknowledge two limitations with the present experiment. The first is related to the simulation technique used whereby frames were shortened by inserting delays and, therefore, the activity concentration may not represent the true count average over the original frame duration. This strategy has the potential to change the mid-times of the time-activity curves and therefore bias kinetic modelling. However, in order to limit the impact of this limitation, all delays were consistently inserted at the start of the frames thereby ensuring that, if a bias was present, it would be consistent within all the datasets and minimally affect the quantitative results. The second limitations which was noted was that this experiment was only conducted in datasets reconstructed with OSEM. While no other algorithms were explored in this study, they will be in future work.

Abbreviations

ADHD	Attention deficit hyperactivity disorder
ALARA	As low as reasonably achievable
ALARP	As low as reasonably practicable
ASD	Autism spectrum disorder
BPD	Bipolar disorder
BP_{ND}	Binding potential relative to non-displaceable volume
CV	Coefficient of variation
DFOV	Display field of view
DSM	5_Diagnostic and Statistical Manual of Mental Disorders fifth edition
FSPGR	Fast spoiled gradient-echo sequence
GCP	Good clinical practice
ICRP	International Commission on Radiological Protection
ID	Intellectual disability
MR	Magnetic resonance
NDDs	Neurodevelopmental disorders
NHS	National Health Service
PET	Positron emission tomography

SDG	Sustainable development goal
SRTM	Single reference tissue model
SUV_R	Standard uptake volume ratio
TACs	Time activity curves
TOF	Time-of-flight

Supplementary Information

The online version contains supplementary material available at https://doi.org/10.1186/s40658-026-00850-y.

Supplementary Material 1.

Acknowledgements
The authors would like to acknowledge the patients that devoted their time and willingness to participate in the original studies. Moreover, DR would like to acknowledge the Chief Investigators for both studies for their willingness to collaborate on this project.

Author contributions
DR, WH and SH are responsible for study conception and design. OH, RM and MN are responsible for the submission of the original protocol to relevant entities (ARSAC, REC, HRA), day to day tasks and management of the study (1) DN, DE and CA are responsible for the submission of the original protocol to relevant entities (ARSAC, REC, HRA), day to day tasks and management of the study (2) DR was also responsible for data collection and analysis. All authors contributed equally to data interpretation and manuscript drafting. All authors read and approved the final manuscript.

Funding
There was no funding available to perform this project.

Data availability
The datasets generated and/or analysed during the current study are not publicly available are available from the corresponding author on reasonable request.

Declarations

Ethics approval and consent to participate
The original studies adhered to the principles outlined in the NHS Research Governance Framework for Health and Social Care (2nd edition), the Declaration of Helsinki and Good Clinical Practice (GCP). They were conducted in compliance with the Protocol, the Data Protection Act and other regulatory requirements and Standard Operating Procedures (SOPs), as appropriate. The data that was used in this project was acquired after the participant's consent was obtained for the original studies (Study 1: REC reference 12/LO/1955, IRAS Project ID 103938; Study 2: REC reference 21/LO/0397, IRAS Project ID 286308). Use of this data was covered in the original consent form, which stated that the data acquired could be used in future related research.

Consent for publication
All patients consented to undergo the original study.

Competing interests
The authors declare that they have no competing interests.

Received: 5 March 2025 / Accepted: 27 February 2026
Published online: 10 March 2026

References

1. Rogeau A, Boer AJ, Guedj E, Sala A, Sommer IE, Veronese M, et al. EANM perspective on clinical PET and SPECT imaging in schizophrenia-spectrum disorders: a systematic review of longitudinal studies. Eur J Nucl Med Mol Imaging [Internet]. 2025;52:876–99. https://doi.org/10.1007/s00259-024-06987-1.
2. NHS England - Transformation Directorate. Precision medicine. 2020 [cited 2024 Jun 2]; https://transform.england.nhs.uk/ai-lab/explore-all-resources/understand-ai/precision-medicine/. Accessed 2 Jun 2024.
3. Ahn B-C. Nuclear Medicine in the Era of Precision Medicine. Nucl Med Mol Imaging [Internet]. 2017;51:99–100. https://doi.org/10.1007/s13139-017-0478-5.
4. Fabritius G, Brix G, Nekolla E, Klein S, Popp HD, Meyer M, et al. Cumulative radiation exposure from imaging procedures and associated lifetime cancer risk for patients with lymphoma. Sci Rep [Internet]. 2016;6:35181. https://doi.org/10.1038/srep35181.
5. Mullin AP, Gokhale A, Moreno-De-Luca A, Sanyal S, Waddington JL, Faundez V. Neurodevelopmental disorders: mechanisms and boundary definitions from genomes, interactomes and proteomes. Transl Psychiatry [Internet]. Nat Publishing Group. 2013;3:e329–329. https://doi.org/10.1038/tp.2013.108.
6. Morris-Rosendahl DJ, Crocq M-A. Neurodevelopmental disorders-the history and future of a diagnostic concept. Dialogues Clin Neurosci [Internet] Les Laboratoires Servier. 2020;22:65–72. https://doi.org/10.31887/DCNS.2020.22.1/macrocq.

7. Alexander RT, Langdon PE, O'Hara J, Howell A, Lane T, Tharian R, et al. Psychiatry and neurodevelopmental disorders: experts by experience, clinical care and research. Br J Psychiatry [Internet]. 2021;218:1–3. https://doi.org/10.1192/bjp.2020.237. 2020/12/28. Cambridge University Press.
8. Costa PF, Testanera G, Camoni L, Terwinghe C, Bailey EA, Bolus NE, et al. Technologist Approach to Global Dose Optimization. J Nucl Med Technol [Internet]. 2019;47:75. https://doi.org/10.2967/jnmt.118.218131.
9. McCutcheon RA, Brown K, Nour MM, Smith SM, Veronese M, Zelaya F, et al. Dopaminergic organization of striatum is linked to cortical activity and brain expression of genes associated with psychiatric illness. Sci Adv [Internet]. Volume 7. American Association for the Advancement of Science; 2025. p. eabg1512. https://doi.org/10.1126/sciadv.abg1512.
10. Pfaff S, Philippe C, Nics L, Berroterán-Infante N, Pallitsch K, Rami-Mark C, et al. Toward the Optimization of (+)-[11 C]PHNO Synthesis: Time Reduction and Process Validation. Volume 2019. Wiley, Ltd;; 2019. p. 4292596. https://doi.org/10.1155/2019/4292596. Contrast Media Mol Imaging [Internet].
11. Tziortzi AC, Searle GE, Tzimopoulou S, Salinas C, Beaver JD, Jenkinson M, et al. Imaging dopamine receptors in humans with [11 C]-(+)-PHNO: Dissection of D3 signal and anatomy. Neuroimage [Internet]. 2011;54:264–77. https://doi.org/10.1016/j.neuroimage.2010.06.044.
12. Bendlin BB, DiFilippo AH, Betthauser TJ, Chin NA, Murali D, Vogt NM, et al. Synaptic vesicle protein SV2A imaging with [11 C]UCB-J as a novel biomarker of neurodegeneration in Alzheimer's disease. Alzheimer's & Dementia [Internet]. Volume 16. John Wiley & Sons, Ltd; 2020. p. e037789. https://doi.org/10.1002/alz.037789.
13. Mansur A, Rabiner EA, Comley RA, Lewis Y, Middleton LT, Huiban M, et al. Characterization of 3 PET Tracers for Quantification of Mitochondrial and Synaptic Function in Healthy Human Brain: 18F-BCPP-EF, 11 C-SA-4503, and 11 C-UCB-J. J Nuclear Med [Internet]. 2020;61:96. https://doi.org/10.2967/jnumed.119.228080.
14. Ribeiro D, Hallett W, Howes O, McCutcheon R, Nour MM, Tavares AAS. Assessing the impact of different penalty factors of the Bayesian reconstruction algorithm Q.Clear on in vivo low count kinetic analysis of [11 C]PHNO brain PET-MR studies. EJNMMI Res [Internet]. 2022;12:11. https://doi.org/10.1186/s13550-022-00883-1.
15. Arora JS. Chapter 20 - Additional Topics on Optimum Design. In: Arora JS, editor. Introduction to Optimum Design (Third Edition) [Internet]. Boston: Academic; 2012. pp. 731–84. https://doi.org/10.1016/B978-0-12-381375-6.00029-2.
16. Riffenburgh RH, Gillen DL. 27 - Techniques to Aid Analysis. In: Riffenburgh RH, Gillen DL, editors. Statistics in Medicine (Fourth Edition) [Internet]. Academic Press; 2020. pp. 631–49. https://doi.org/10.1016/B978-0-12-815328-4.00027-9
17. Adachi M, Hosoya T, Haku T, Yamaguchi K, Kawanami T. Evaluation of the Substantia Nigra in Patients with Parkinsonian Syndrome Accomplished Using Multishot Diffusion-Weighted MR Imaging. AJNR Am J Neuroradiol. 1999;1500–6.
18. GE Healthcare, SIGNA™, PET/MR Technical Data. 2014 [cited 2024 Jun 9]; https://promed-sa.com/wp-content/uploads/2020/08/PET-MR_Datasheet_DOC1545629.pdf. Accessed 9 Jun 2024.
19. Hansson SO. Chapter 9 - ALARA: What is Reasonably Achievable? In: Oughton D, Hansson SO, editors. Radioactivity in the Environment [Internet]. Elsevier; 2013. pp. 143–55. https://doi.org/10.1016/B978-0-08-045015-5.00009-5.
20. Mattsson S, Johansson L, Leide Svegborn S, Liniecki J, Noßke D, Riklund KÅ et al. ICRP Publication 128: Radiation Dose to Patients from Radiopharmaceuticals: a Compendium of Current Information Related to Frequently Used Substances. Ann ICRP [Internet]. SAGE Publications Ltd; 2015;44:7–321. https://doi.org/10.1177/0146645314558019
21. Currie GM, Hawk KE, Rohren EM. Challenges confronting sustainability in nuclear medicine practice. Radiography [Internet]. 2024;30:1–8. https://doi.org/10.1016/j.radi.2024.04.026. .
22. Rühm W, Applegate K, Bochud F, Laurier D, Schneider T, Bouffler S, et al. The system of radiological protection and the UN sustainable development goals. Radiat Environ Biophys [Internet]. 2024. https://doi.org/10.1007/s00411-024-01089-w.

Publisher's Note